



ELSEVIER

Ultramicroscopy 86 (2001) 207–215

ultramicroscopy

www.elsevier.nl/locate/ultramic

Thermomechanical noise of a free v-shaped cantilever for atomic-force microscopy

Robert W. Stark*, Tanja Drobek, Wolfgang M. Heckl

Universität München, Institut für Kristallographie und Angewandte Mineralogie, Theresienstr. 41, 80333 München, Germany

Received 31 May 2000

Abstract

We have calculated the thermal noise of a v-shaped AFM cantilever (Microlever, Type E, Thermomicroscopes) by means of a finite element analysis. The modal shapes of the first 10 eigenmodes are displayed as well as the numerical constants, which are needed for the calibration using the thermal noise method. In the first eigenmode, values for the thermomechanical noise of the z -displacement at 22°C temperature of $\sqrt{\langle u_1^2 \rangle} = 0.627 \text{ \AA} / \sqrt{c_{\text{cant}}}$ and the photodiode signal (normal-force) of $\sqrt{\langle S_1^2 \rangle} = 0.558 \text{ \AA} / \sqrt{c_{\text{cant}}}$ were obtained. The results also indicate a systematic deviation of the spectral density of the thermomechanical noise of v-shaped cantilevers as compared to rectangular beam-shaped cantilevers. © 2001 Elsevier Science B.V. All rights reserved.

PACS: 61.16.Ch; 07.79.Lh; 07.10.Cm; 43.40.Hb

Keywords: Atomic-force microscopy

1. Introduction

The micromechanical cantilevers commonly used in atomic-force microscopy (AFM) are forced to non-negligible thermomechanical oscillations already at room temperature. These oscillations impose a fundamental restriction to the accuracy of force detection in AFM [1–3]. A similar limit of sensitivity in force detection is encountered in experimental setups for the detection of gravitational waves (e.g. Ref. [4] and references therein). However, the thermally driven oscillations can be

analyzed in order to obtain information on the tip-sample interaction. It was shown, that thermomechanical noise allows for the determination of oscillatory hydration potentials [5] as well as the measurement of viscoelastic properties of polymers [6,7].

Another very common application of thermomechanical noise analysis is the fast and non-destructive calibration of the cantilever spring constant [8–13]. Present theoretic descriptions of thermomechanically induced noise in AFM measurements assume a rectangular geometry of the cantilever [10,14,15]. In practical AFM applications, very often v-shaped cantilevers are used as force sensors, for example in the magnetically driven intermittent contact mode [16,17]. The so-called parallel beam approximation (PBA) was

*Corresponding author. Tel.: +49-89-23944340; fax: +49-89-23944331.

E-mail address: robert@nanomanipulation.de (R.W. Stark).

introduced as an analytical estimation of the spring constant [18]. A more sophisticated analytical approach was found to yield comparable results to a finite element analysis (FEA) [19]. Later, an improved PBA was suggested [20], which was in very good agreement with finite element calculations. Finite element calculations were also performed in order to explain special features encountered in force curve measurements [21]. In order to account for the metal coating of ceramic cantilevers detailed FEA simulations were carried out [22]. Further FEA calculations were performed in order to understand image formation in different types of overtone microscopy [23,24].

However, the “first principle” finite element calculations are hampered with the fact, that already small deviations from the assumed geometric data, e.g. due to a ill-defined thickness of the metal coating or a distortion in the cantilever geometry caused by a mask misalignment, can lead to significant systematic discrepancies between the real spring constant and the calculated value.

Thus, a hybrid calibration method is desirable that combines the advantages of the FEA-approach with the benefits of thermal noise analysis. In this paper, the thermomechanical noise of a v-shaped cantilever is investigated theoretically by means of a finite element analysis. The results for the unrestricted cantilever allow to calculate a calibration table for the determination of the cantilever spring by the thermal noise method.

2. Outline of theory

2.1. Thermomechanical noise

In thermodynamic equilibrium the mean-square displacement of the tip from its neutral position is described by

$$\sqrt{\langle u^2 \rangle} = \sqrt{\frac{k_B T}{c_{\text{cant}}}}. \quad (1)$$

Here, u is the z -displacement of the tip, k_B is the Boltzmann constant, T the temperature of the surrounding heat bath, c_{cant} the cantilever spring

constant, and $\langle \cdot \rangle$ denotes the average in time (cf. e.g. [8]). Note that this formula is independent of the cantilever geometry.

However, when light-lever detection is used for the displacement measurement, experimental noise-data cannot be analyzed applying Eq. (1) directly. In order to calculate the photodiode signal in a light-lever setup, the shape of the transverse vibrational modes must be known to correct for geometric effects. Eq. (1) has to be corrected for the bandwidth limitation of the detection system as well.

2.2. Multiple degrees of freedom

For a mathematical description of the cantilever dynamics in a frequency range above the fundamental frequency the cantilever must be modelled as a multiple-degree-of-freedom system. In the following, only a brief review of the basic ideas is given, a more thorough treatment can be found in textbooks on structural dynamics (e.g. Refs. [25,26]).

A discrete finite element approach is used in order to describe a cantilever with arbitrary geometry. In the matrix formalism, the equation of motion is

$$\mathbf{M}\ddot{\mathbf{u}}(t) + \mathbf{c}\dot{\mathbf{u}}(t) + \mathbf{K}\mathbf{u}(t) = 0, \quad (2)$$

where \mathbf{M} is the mass matrix, \mathbf{K} the stiffness matrix, $\mathbf{u}(t)$ the vector of the nodal displacements, and \mathbf{c} the damping matrix. The eigenvalue problem is solved in order to determine the resonant frequencies and the eigenmodes. This yields the eigenvectors Φ_n and the eigenfrequencies ω_n . The eigenmodes can be used as base vectors of a generalized coordinate system, where it is possible to separate the time and space dependence of the cantilever motion.

For the transformation into generalized displacement coordinates $q_n(t)$ the transformation rule

$$\mathbf{u}(t) = \sum_n \Phi_n q_n(t) \quad (3)$$

is applied to Eq. (2). After a straightforward calculation (cf. e.g. Refs. [25,26]), a set of ordinary differential equations is obtained

$$\mathbf{M}_n \ddot{q}_n(t) + \mathbf{C}_n \dot{q}_n(t) + \mathbf{K}_n q_n(t) = 0. \quad (4)$$

Here, $M_n = \Phi_n^T \mathbf{M} \Phi_n$ is the generalized mass, $K_n = \Phi_n^T \mathbf{K} \Phi_n$ the generalized spring stiffness, and $C_n = \Phi_n^T \mathbf{c} \Phi_n$ the generalized damping. For the damping it is more convenient to use the modal damping coefficient $\gamma_n = C_n/2\omega_n M$. For the sake of simplicity, we will assume Rayleigh damping, leading to the relation

$$\gamma_n = \frac{a_0}{2\omega_n} + \frac{a_1 \omega_n}{2}, \quad (5)$$

where a_0 and a_1 are the mass proportional and the stiffness proportional damping, respectively (for more details cf. e.g. Refs. [25,27]). With this assumption, Eqs. (4) represent a set of decoupled ordinary differential equations.¹

In the case of a constant mass density of the structure and orthonormal Φ_n , the generalized mass equals the total mass

$$M_n = \Phi_n^T \mathbf{M} \Phi_n = M. \quad (6)$$

The generalized spring stiffness is then

$$K_n = M\omega_n^2. \quad (7)$$

Treating the cantilever as a system of N harmonic oscillators in thermodynamic equilibrium, the mean-square displacement of the individual generalized oscillators is given by

$$\langle q_n^2 \rangle = \frac{k_B T}{K_n}. \quad (8)$$

Note that the K_n are not equal to the (quasistatic) spring constant c_{cant} .

The average potential energy of the cantilever in thermal equilibrium is given by

$$\langle U_{\text{cant}} \rangle = \frac{1}{2} c_{\text{cant}} \langle u^2 \rangle = \frac{1}{2} k_B T. \quad (9)$$

The fraction of average potential energy of the j th node of the cantilever found in the n th eigenmode can be determined from

$$C_{n,j} = \Phi_{n,j}^2 \left/ \frac{K_n}{c_{\text{cant}}} \right. \quad (10)$$

The quasistatic spring constant c_{cant} is determined by a static structural analysis. For the calculation of tip displacement a node j is chosen at the tip. The value $C_{n,j}$ represents the percentage of energy

of the multiple-degree-of-freedom system found in the n th eigenmode.

It is worth to note that other generalized coordinate systems could be used as well. In commercial finite element software, e.g. the Φ_n are normalized by the condition $\hat{\Phi}_n^T \mathbf{M} \hat{\Phi}_n = 1$ (e.g.²). Eq. (10) in this coordinate system transforms into $C_{n,j} = \hat{\Phi}_{n,j}^2 / m / K_n / c_{\text{cant}} = \hat{\Phi}_{n,j}^2 / \omega_n^2 / c_{\text{cant}}$. However, since the choice of the generalized coordinate system is arbitrary, identical numerical results are obtained. A more detailed treatment can be found in Ref. [28].

In order to account for the light-lever detection scheme, another correction factor has to be introduced:

$$C_{n,j}^{\text{det}} = \left[\frac{\partial_x \Phi_{n,j}}{\partial_x \Psi_j} \right]^2. \quad (11)$$

This factor is the ratio of the geometrical derivative of the dynamic bending shape $\partial_x \Phi_{n,j}$ of the n th eigenmode and the quasistatic bending shape $\partial_x \Psi_j$ at the node j . It can be understood as a geometric enhancement factor that correlates the photodiode signal obtained from an oscillating cantilever to the photodiode calibration (deflection vs. signal) obtained by a quasistatic force curve. For eigenmodes with $C_{n,j}^{\text{det}} > 1$, the photodiode signal is increased as compared to a quasistatic deflection, if $C_{n,j}^{\text{det}} < 1$ the photodiode signal is decreased. Applying the definition of Eq. (11), $C_{n,j}^{\text{det}}$ corrects for the light-lever detection of a point-like laser spot, whereas finite spot size and the limited bandwidth of the detection system are not included.

Both parameters $C_{n,j}$, and $C_{n,j}^{\text{det}}$ are independent of the material parameters, mass density ρ and the Young's modulus E , since they enter as linear factors into the mass or stiffness matrix and can therefore be cancelled.

2.3. Spectral power density

For a general continuous multimode system, the spectral power density was given in Ref. [4]. A detailed discussion for rectangular AFM cantilevers can be found in Ref. [14]. In a similar

¹Note that non-proportional damping can lead to a damping matrix that cannot be diagonalized. This would lead to coupling of the different eigenmodes.

²Anslys 5.4 (Ansys Inc., Canonsburg, PA, USA, 1998).

approach, the displacement of the j th node in the n th mode for a discrete multiple-degree-of-freedom system is obtained by

$$\langle u_n^2(\omega) \rangle_j = \Phi_{n,j}^2 \frac{2k_B T}{m} \frac{\gamma_n/m}{(\omega_n^2 - \omega^2)^2 + (\omega\gamma_n/m)^2}, \quad (12)$$

and the root-mean-square photodiode signal measured at node j is

$$\langle S_n^2(\omega) \rangle_j = C_{n,j}^{\text{det}} \Phi_{n,j}^2 \frac{2k_B T}{m} \frac{\gamma_n/m}{(\omega_n^2 - \omega^2)^2 + (\omega\gamma_n/m)^2}. \quad (13)$$

Often the quality factor Q_n is used instead of a damping coefficient γ_n , thus

$$\gamma_n/m = \omega_n/Q_n \quad (14)$$

has to be applied then. By integration, the modal thermomechanical deflection and the photodiode signal can be calculated:

$$\langle u_n^2 \rangle_j = \frac{1}{2\pi} \int_{-\infty}^{\infty} \langle u_n^2(\omega) \rangle_j d\omega, \quad (15)$$

$$\langle S_n^2 \rangle_j = \frac{1}{2\pi} \int_{-\infty}^{\infty} \langle S_n^2(\omega) \rangle_j d\omega. \quad (16)$$

With an additional weighting factor in Eqs. (15) and (16), the transfer function of the detection system could also be included.

The mean square of the deflection and the photodiode signal of the N -oscillator cantilever at node j is obtained from

$$\langle u^2 \rangle_j = \sum_{n=1}^N \langle u_n^2 \rangle_j, \quad (17)$$

$$\langle S^2 \rangle_j = \sum_{n=1}^N \langle S_n^2 \rangle_j. \quad (18)$$

In the following, the index j will be suppressed. By convention, we choose a node of the model at the rear side of the cantilever just above the AFM tip as indicated in Fig. 1(a).

3. Results and discussion

In order to obtain accurate geometric data for the finite element modelling, the cantilever [gold-coated sharpened microlever, type E, Thermomicroscopes, Sunnyvale CA, USA] was analyzed by

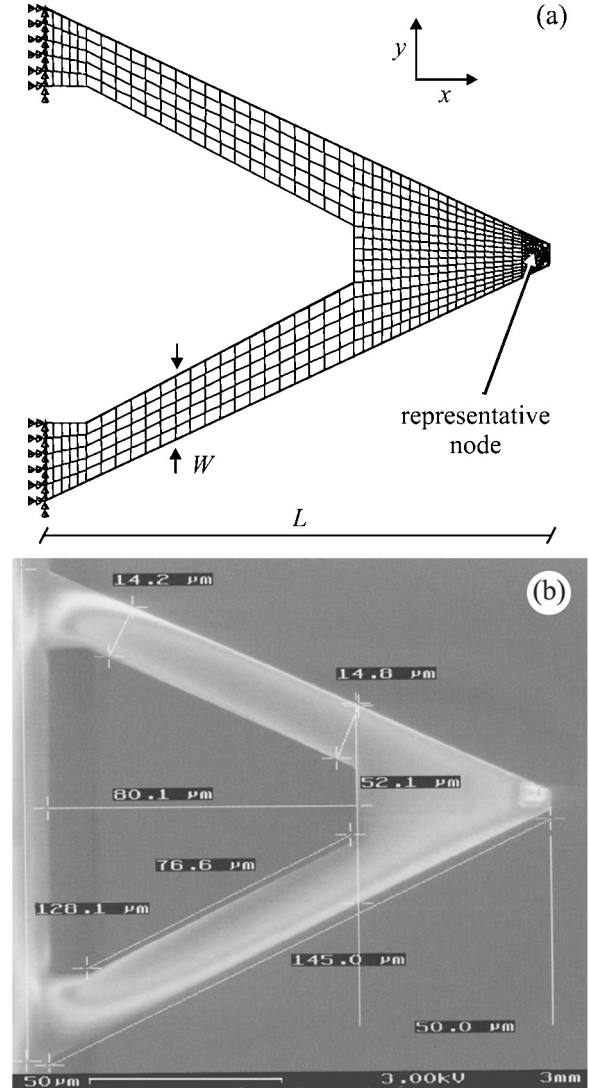


Fig. 1. (a) Mesh of the AFM cantilever used for the finite element analysis (FEA). The arrows at the cantilever base represent the restrictions of the nodal degrees of freedom. The large arrow points at a node which was chosen in order to calculate the nodal deflection. (b) Scanning electron micrograph of the cantilever. The geometric data were used for the FEA as indicated. (Gold-coated sharpened microlever, type E, Thermomicroscopes).

scanning electron microscopy. Resonant frequencies and damping coefficients were measured by analysis of the thermomechanical noise in the photodiode signal. The cantilever thickness was

determined from an edge-on micrograph (data not shown). A gold film thickness of 60 nm was measured by AFM imaging of an edge prepared by partially removing the gold layer from the cantilever chip. From the electron microscopy and AFM data (Fig. 1(b)) the finite element mesh was modelled (Fig. 1(a)) with a length of $L = 132 \mu\text{m}$, a width of $W = 16.2 \mu\text{m}$, and a thickness of $T = 0.63 \mu\text{m}$ (nominal values: $L = 140 \mu\text{m}$, $W = 18 \mu\text{m}$, $T = 0.6 \mu\text{m}$).

The finite element analysis (FEA) was carried out by the use of a commercial software ANSYS 5.4 (see footnote 2) running on an IBM-SP2 workstation at Leibniz Rechenzentrum, München Germany. The model of the cantilever geometry was built up with brick elements (solid-type 73). A mesh of 2272 nodes was used for the calculations. The mesh independence was demonstrated by further mesh refinement.

The silicon–nitride/gold system was replaced by a one-component model using effective values for the mass density, the Young's modulus, and the Poisson ratio following a procedure similar to the method suggested by Hazel and Tsukruk [22]. The effective Young's modulus was set to $E = 140 \text{ GPa}$. In order to match the experimental resonant frequencies of the symmetric as well as antisymmetric modes, the Poisson ratio ν of the bi-component system was set to an effective value of $\nu = 0.4$.

The quasistatic spring constant as obtained from a static FEA is $c_{\text{cant}} = 0.13 \text{ N/m}$ (manufacturer's value: $c_{\text{cant}} = 0.10 \text{ N/m}$). From a variation of the thickness in the range from $T = 100$ to 1000 nm the empirical relation $c_{\text{cant}} = 1.054 T^3$ (with T in μm) was found to be a good approximation. Additionally, c_{cant} is directly proportional to the material parameter Young's modulus E . Thus, already the simple analytic PBA [cf. Ref. [18] Eq. (9), Ref. [20] Eq. (9)]

$$c_{\text{cant}} = \frac{ET^3W}{2L^3} = 0.12 \text{ N/m} \quad (19)$$

is a good approximation and differs only 5% from the values obtained by the numerical FEA.

The modal shapes of the first ten transversal eigenmodes obtained by the modal analysis tool (see footnote 2) are displayed in Fig. 2, the

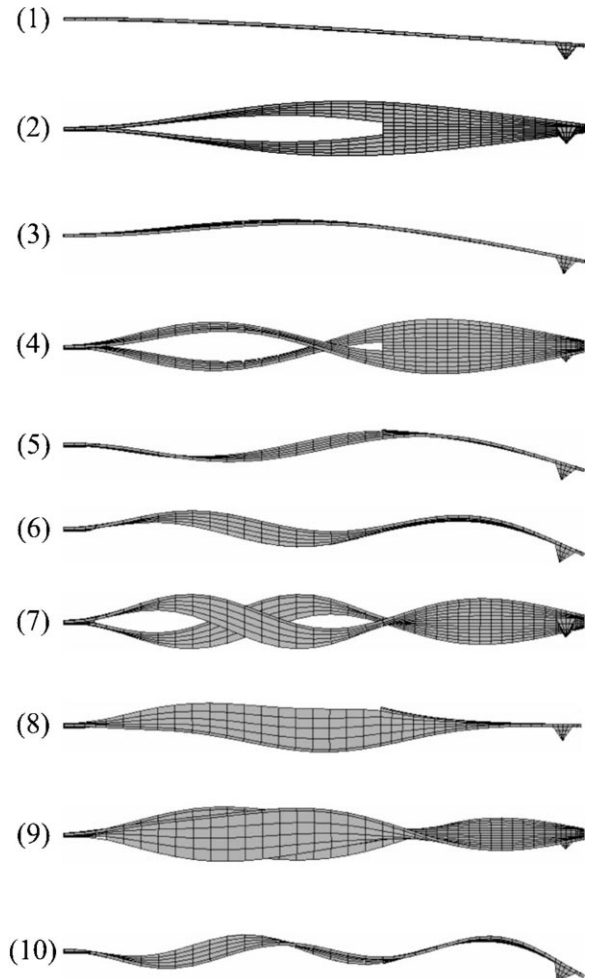


Fig. 2. The first ten eigenmodes of a v-shaped cantilever (sideview). They can be classified into symmetric (1, 3, 5, 6, 8, 10) and antisymmetric (2, 4, 7, 9) modes. Only symmetric modes yield a normal-force photodiode signal.

respective eigenfrequencies are given in Table 1. The eigenmodes can be classified into two categories, symmetric and antisymmetric modal shapes. In the symmetric modes the (x - z) plane is a mirror plane, whereas the antisymmetric modes are antisymmetric to the x -direction. From a geometric point of view, some of the symmetric eigenmodes (1, 3, 5, 6, 10) correspond to the first five eigenmodes of a rectangular beam (B1, B2, B3, B4, B5, e.g. [10]) respectively. Note that in this communication the eigenmodes of a beam are

Table 1

Summary of cantilever data. The coefficients C_n give the fraction of energy in the respective mode [cf. Eq. (10)]. Deviations of $\sum C_n$ from the ideal value of 1.000 are caused by intrinsic numerical errors. The respective geometric amplification of the photodiode signal can be calculated from $\sqrt{C_n^{\text{det}}}$ [cf. Eq. (11)]

Mode n	Frequency (kHz)	C_n	C_n^{det}
1	38.8	0.963	0.79
2	192.3	0.000	7.26
3	203.1	0.036	8.26
4	540.1	0.000	22.41
5	545.2	0.004	24.17
6	1054.5	0.001	60.58
7	1068.7	0.000	66.55
8	1217.3	0.001	24.17
9	1507.2	0.000	56.44
10	1698.3	0.000	136.45

numbered by Bn in order to avoid confusion with the eigenmodes of the v-shaped cantilever labelled n . The first three antisymmetric modes (2, 4, 7) correspond to torsional eigenmodes of a rectangular beam. These modes do not contribute to the thermal noise in the z -displacement of the tip, since there the tip oscillates parallel to the sample surface. However, for the eigenmodes (8) and (9) of the v-shaped cantilever there are no corresponding eigenmodes of a simple rectangular beam. In these modes, both arms of the cantilever vibrate independently from the baseplate. In the symmetric vibration mode (8) both arms vibrate parallel resulting in a motion similar to a bird beating its wings. In the antisymmetric mode (9) both arms twist.

The spectral density of the thermomechanical fluctuations is plotted in Fig. 3 [cf. Eqs. (12), (13), summation over n]. The plot was generated using the experimental Q -factors $Q_1 = 60$ and $Q_5 = 340$. The other Q -factors were calculated using Eqs. (5) and (14). The noise in the tip z -deflection (solid) decreases much more rapidly with increasing frequency as compared to the noise measured by a light-lever setup (dashed). This is caused by the geometric enhancement of the higher eigenmodes ($C_n^{\text{det}} > 1$ for $n > 1$).

Table 1 gives a summary of the eigenfrequencies, the correction factors C_n and the detection factors C_n^{det} . The factors C_n and C_n^{det} are insensitive to deviations in the cantilever geometry. A

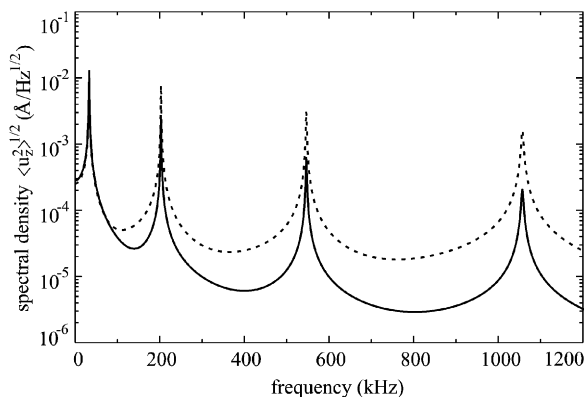


Fig. 3. Spectral density of the thermomechanical fluctuations of the tip-position $\sqrt{u_z}$ (solid) and the normal-force photodiode signal \sqrt{S} (dashed) for a resolution bandwidth of 1 Hz.

variation in L of $\delta L = 10\%$ causes a relative variation of $\delta C_n < 2\%$ and $\delta C_n^{\text{det}} < 3\%$, whereas the respective eigenfrequencies may vary more than 20%. Therefore, in comparison to typical experimental errors, there is only a small deviation from the theoretic energy distribution for the thermomechanical noise as derived from Eq. (10) due to variations of the cantilever geometry.

Alternatively, the numerical results from Table 1 can be validated by checking the numerical model for energy conservation. The energy “loss” or “gain” of the model due to intrinsic numerical

errors and the finite number of modes is given by $\delta U_{\text{num}} = \sum_1^{10} C_n^{\text{eff}} - 1$. Here, the “energy gain” of the numerical model is $\delta U_{\text{num}} \approx 0.5\%$. This means, that the numerical errors in the energy distribution among the eigenmodes can be estimated to be smaller than 1%.

Table 2 summarizes the normalized thermomechanical deflection of the tip in the z-direction attributed to the different eigenmodes. For comparison, also the values for a rectangular cantilever beam are given for geometrically equivalent eigenmodes (same number of nodes). The thermomechanical noise as it would be measured in the normal-force photodiode signal is listed in Table 3.

The actual values for cantilevers can be calculated by division with $\sqrt{c_{\text{cant}}}$.

Note that there is a deviation of 3.4% for the thermomechanical noise measured in the photodiode signal for the v-shaped cantilever as compared to the rectangular cantilever beam. Thus, for this type of v-shaped cantilevers, spring constants determined by a naive use of the thermal noise method under the simplifying assumption of a rectangular beam model can be expected to be systematically 7% too large.

Finally, the limitations of the combined FEA – thermal noise approach presented here, should be discussed briefly. A deviation of the modal shape

Table 2

Thermomechanical noise of the tip deflection $\sqrt{\langle u_n^2 \rangle}$ of a beam like [10] and a v-shaped cantilever at 22°C. The values are normalized to a spring constant of 1 N/m. A transformation to other spring constants is done by dividing with $\sqrt{c_{\text{cant}}}$

Mode	Beam ^a (Å)	Mode	v-shape (Å)
B1	0.629	1	0.627
—	—	2	0.000
B2	0.100	3	0.121
—	—	4	0.000
B3	0.036	5	0.042
B4	0.018	6	0.021
—	—	7	0.000
—	—	8	0.019
—	—	9	0.000
B5	0.011	10	0.012

^aFrom Table 1 in Ref. [10].

Table 3

Thermomechanical noise of the photodiode signal $\sqrt{\langle S_n^2 \rangle}$ of a beam-like [10] and a v-shaped cantilever at 22°C. The values are normalized to a spring constant of 1 N/m. A transformation to other spring constants is done by dividing with $\sqrt{c_{\text{cant}}}$

Mode	Beam ^a (Å)	Mode	v-shape (Å)
B1	0.577	1	0.558
—	—	2	0.000
B2	0.320	3	0.348
—	—	4	0.000
B3	0.188	5	0.206
B4	0.134	6	0.172
—	—	7	0.000
—	—	8	0.092
—	—	9	0.000
B5	0.104	10	0.144

^aFrom Table 1 in Ref. [10].

of a real cantilever from the theoretic model can be expected from the multilayer structure of the cantilever that consists of a Si_3N_4 ceramics covered with a reflective gold layer. Due to the metal coating, the cantilever can be prestressed by the interfacial stress between the gold and the ceramics. For rectangular cantilevers it was shown that there is a slight deviation of experimentally obtained bending shapes as compared to theoretical ones [29]. A similar result must be expected for v-shaped cantilevers. Thus, a conservative estimate of the relative uncertainty of the tip displacement of $\delta\langle u_n^2 \rangle = 5\%$ ($\delta\langle S_n^2 \rangle = 5\%$) seems appropriate due to systematic errors (limited accuracy). This estimate accounts only for numerical errors and deviations of the true cantilever geometry from the FEA modelling. Additional experimental errors may be caused by finite laser spot size, bandwidth limitations, and other effects.

4. Conclusions

A combined method for the calibration of v-shaped cantilevers employing finite-element calculations together with a complementary analysis of the thermomechanical fluctuations is suggested. For a special type of v-shaped cantilever, the thermal noise of the tip deflection and the photo diode signal is calculated (Microlever, Type E, Thermomicroscopes). The modal shapes of the first 10 eigenmodes are given together with the numerical constants that are needed for a calibration using the thermal noise method. Following the procedure described here, similar FEA calculations can easily be carried out in order to provide reliable data for other types of v-shaped cantilevers.

The results also indicate that there is a systematic deviation in the thermomechanical noise of v-shaped cantilevers as compared to rectangular beam-shaped cantilevers. Thus, if a fast and nondestructive calibration for a v-shaped cantilever is needed, a numerical finite element analysis of the cantilever geometry to be calibrated is inevitable.

Acknowledgements

We thank Dr. Heribert Lorenz (Nanotools GmbH) for SEM imaging. Financial support by grant BMBF 13N7509/1 (RWS) and DFG Grant He-1617/7-2 (TD) is gratefully acknowledged.

References

- [1] D. Smith, *Rev. Sci. Instr.* 66 (5) (1995) 3191.
- [2] A. García-Valenzuela, J. Villatoro, *J. Appl. Phys.* 84 (1) (1998) 58.
- [3] F. Gittes, C. Schmidt, *Eur. Biophys. J.* 27 (1998) 75.
- [4] P. Saulson, *Phys. Rev. D* 42 (8) (1990) 2437.
- [5] J. Cleveland, T. Schaffer, P. Hansma, *Phys. Rev. B* 52 (12) (1995) R8692.
- [6] A. Roters, M. Gelbert, M. Schimmel, J. Rühe, D. Johannsmann, *Phys. Rev. E* 56 (3) (1997) 3256.
- [7] M. Gelbert, A. Roters, M. Schimmel, J. Rühe, D. Johannsmann, *Surf. Interface Anal.* 27 (1999) 572.
- [8] J. Hutter, J. Bechhoefer, *Rev. Sci. Instr.* 64 (7) (1993) 1868.
- [9] J. Hutter, J. Bechhoefer, *Rev. Sci. Instr.* 64 (11) (1993) 3342.
- [10] H. Butt, M. Jaschke, *Nanotechnology* 6 (1995) 1.
- [11] E. Florin, M. Rief, H. Lehmann, M. Ludwig, C. Dornmair, V. Moy, H. Gaub, *Biosens. Bioelectr.* 10 (9–10) (1995) 895.
- [12] D. Walters, J. Cleveland, N. Thomson, P. Hansma, M. Wendman, G. Gurley, V. Elings, *Rev. Sci. Instr.* 67 (10) (1996) 3583.
- [13] J. Chon, P. Mulvaney, J. Sader, *J. Appl. Phys.* 87 (8) (2000) 3978.
- [14] M. Salapaka, H. Bergh, J. Lai, A. Majumdar, E. McFarland, *J. Appl. Phys.* 81 (6) (1997) 2480.
- [15] J. Sader, *J. Appl. Phys.* 84 (1) (1998) 64.
- [16] W. Han, S. Lindsay, T. Jing, *Appl. Phys. Lett.* 69 (26) (1996) 4111.
- [17] H. Schindler, D. Badt, P. Hinterdorfer, F. Kienberger, A. Raab, S. Wielert-Badt, V. Pastushenko, *Ultramicroscopy* 82 (1–4) (2000) 227.
- [18] J. Butt, P. Siedle, K. Seifert, K. Fendler, T. Seeger, E. Bamberg, A. Weisenhorn, K. Goldie, A. Engel, *J. Microsc. Oxford* 169 (Jan) (1993) 75.
- [19] J. Neumeister, W. Ducker, *Rev. Sci. Instr.* 65 (8) (1994) 2527.
- [20] J. Sader, *Rev. Sci. Instr.* 66 (9) (1995) 4583.
- [21] M. Sasaki, K. Hane, S. Okuma, Y. Bessho, *Rev. Sci. Instr.* 65 (6) (1994) 1930.
- [22] J. Hazel, V. Tsukruk, *Thin Solid Films* 339 (1999) 249.
- [23] T. Drobek, R. Stark, M. Gräber, W. Heckl, *New J. Phys.* 1 (1999) 15.

- [24] R. Stark, T. Drobek, W. Heckl, *Appl. Phys. Lett.* 74 (22) (1999) 3296.
- [25] R. Clough, J. Penzien, *Dynamics of Structures*, McGraw-Hill, Singapore, 1993, 2nd ed.
- [26] M. Géradin, D. Rixen, *Mechanical Vibrations: Theory and Application to Structural Dynamics*, Wiley, New York, 1997, 2nd ed.
- [27] R. Stark, W. Heckl, *Surf. Sci.* 457 (1–2) (2000) 219.
- [28] R. Stark, *Dynamische und quasistatische Rasterkraftmikroskopie zur Materialcharakterisierung: Theorie und Experiment*, Ph.D. thesis, Universität München, 2000.
- [29] U. Rabe, K. Janser, W. Arnold, *Rev. Sci. Instr.* 67 (9) (1996) 3281.